

A First-Principles Description of Liquid BeF₂ and Its Mixtures with LiF: 2. Network Formation in LiF–BeF₂

Mathieu Salanne, Christian Simon, and Pierre Turq

Université Pierre et Marie Curie-Paris 6, CNRS, ESPCI, UMR 7612, Laboratoire LI2C, Case Courrier 51, 4 Place Jussieu, 75252 Paris Cedex 05, France

Robert J. Heaton and Paul A. Madden*

Chemistry Department, University of Edinburgh, Edinburgh EH9 3JJ, U.K.

Received: February 16, 2006

A polarizable ionic interaction potential, constructed from first-principles calculations, is used to examine the structure, vibrational spectra, and transport properties of molten mixtures of LiF and BeF₂ across a range of compositions. The simulations reproduce the experimentally measured vibrational frequencies of the fluoroberyllate (BeF₄²⁻) ions, which form in the melt, as well as conductivity and viscosity values across the composition range. Examination of the structures of the melts reveals the emergence of a slowly relaxing network of BeF₄ units as the concentration of BeF₂ is increased. The relationship between the appearance of the network and the composition dependence of the transport properties is explored.

I. Introduction

In the preceding paper,¹ we showed how a polarizable interaction potential for BeF₂ could be developed on a purely first-principles basis, and we compared simulation results obtained with it with measured properties of the pure material. In fact, this potential was obtained by *simultaneously* fitting ab initio information for various condensed-phase configurations of BeF₂ and LiF, though, of course, only the Be–F, F–F, and Be–Be parts of the potential were relevant to the previous study. The properties of a very similar potential for LiF were described elsewhere.² In this paper, we will make use of the full potential and describe comparisons between calculated values for experimentally observable properties of LiF–BeF₂ mixtures and those obtained from real experiments. We described the significance of these and similar mixtures in proposed nuclear technologies in the Introduction to that paper. As we also noted there, an extensive experimental database for these materials exists, as a legacy of the Molten Salt Reactor program, so that they provide an excellent testing ground for the ab initio modeling capability for fluorides we are developing.

One advantage of working with the mixtures, rather than pure BeF₂, is that it is possible to carry out simulations in a temperature range that overlaps one in which experiments have been performed. In pure BeF₂, most experiments have been performed at temperatures where the melt is so viscous that we cannot equilibrate it even in very long simulations. As will be shown, the comparison of predicted and measured properties suggests that the potential is predicting excellent values for observables, even though no information about the mixtures was included in the dataset on which the potential was constructed, only information on the pure materials. Armed with this reassurance, we will then analyze the local structures of the simulated mixtures and, in particular, the formation of different complex ion species (BeF₄²⁻, Be₂F₇³⁻, etc.), and ultimately, an extended network as the BeF₂ concentration is increased. Equilibria between these species have been proposed, notably

by Baes,³ to account for the variation of the thermodynamic properties of the ions and the transport properties of the melts as the composition is changed. In the final section, we will consider the relationship between the developing network structure of the melt and the transport properties from a microscopic perspective.

II. Transport Properties of LiF–BeF₂ Mixtures, Comparison with Experiment

We have carried out simulations for mixtures of compositions with 50% LiF (i.e., LiBeF₃), 54.4% LiF, 58.8% LiF, 66.6% LiF (i.e., Li₂BeF₄), and 75% LiF (Li₃BeF₅). These compositions span the range for which the mixture has a reasonably low viscosity for temperatures below 1000 K and lie close to the eutectic composition (46.9% LiF). For compositions richer in BeF₂, the mixture becomes extremely viscous, and for those richer in LiF, the liquidus becomes very high. A phase diagram is given in ref 4. All of the systems were studied at 873 K, except the 75% LiF mixture, which was simulated at 1073 K. The temperature effects were studied on Li₂BeF₄, for which additional simulations were carried out at 773, 828, 923, and 973 K. The simulations involved around 500 ions, depending on composition, and lasted for up to 5 million MD steps in order to calculate good values for the electrical conductivity and viscosity. The full potential was specified in the appendix to the previous paper. The simulations were equilibrated in NPT runs with zero external pressure; in all cases, this resulted in densities within 0.5% of the experimental values.⁵

A. Electrical Conductivity and Diffusion Coefficients. The electrical conductivity of these melts is relatively easy to measure, and a very extensive set of results is available.⁶ In the computer simulation, we obtain the conductivity from the long-time slope of a plot of the mean-squared displacement of the charge versus time,⁷

$$\lambda = \frac{\beta e^2}{V} \lim_{t \rightarrow \infty} \frac{1}{6t} \langle |q_{\text{Be}} \Delta_{\text{Be}}(t) + q_{\text{Li}} \Delta_{\text{Li}}(t) + q_{\text{F}} \Delta_{\text{F}}(t)|^2 \rangle \quad (1)$$

* Corresponding author. E-mail: p.madden@ed.ac.uk.

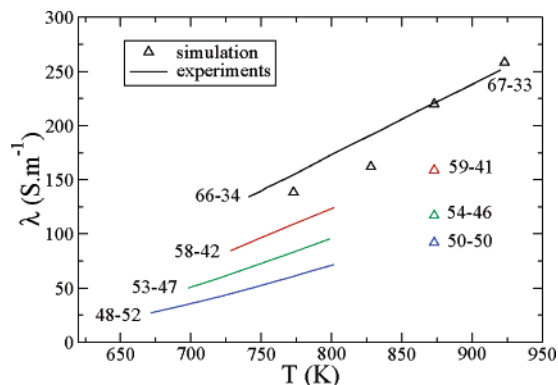


Figure 1. Experimental and simulated electrical conductivity for various LiF–BeF₂ melts as a function of temperature.

where q_α is the charge of an ion of species α , and $\Delta_\alpha(t)$ is the displacement of all the ions of that species in time t

$$\Delta_\alpha(t) = \sum_{i \in \alpha} \delta \mathbf{r}_i(t) \quad (2)$$

Here $\delta \mathbf{r}_i(t)$ is the displacement of individual ion i .

The values obtained for the different LiF–BeF₂ melts are given in Figure 1, where the corresponding experimental values are also indicated. We can see that the agreement between the calculated values and the extrapolated analytical representations of the experimental data is very good, even if most of the experimental results correspond to lower temperatures than where calculations were undertaken. The good agreement over a broad range of compositions is a good indicator of the validity of the simulation models.

The expression for the conductivity can be approximated by neglecting the correlations between the displacements of different ions, i.e.,

$$\langle \delta \mathbf{r}_i(t) \cdot \delta \mathbf{r}_j(t) \rangle = 0, \quad i \neq j \quad (3)$$

This leads to the Nernst–Einstein approximation for the conductivity

$$\lambda^{\text{NE}} = \frac{\beta e^2}{V} (\rho_{\text{Be}} q_{\text{Be}}^2 D_{\text{Be}} + \rho_{\text{Li}} q_{\text{Li}}^2 D_{\text{Li}} + \rho_{\text{F}} q_{\text{F}}^2 D_{\text{F}}) \quad (4)$$

where ρ_α is the number density of species α . In obtaining this expression, we used the Einstein expression for the diffusion coefficient

$$D_\alpha = \lim_{t \rightarrow \infty} \frac{\langle |\delta \mathbf{r}_i(t)|^2 \rangle}{6t} \quad (5)$$

The values for the diffusion coefficient for the LiF–BeF₂ (67–33) mixture obtained at several temperatures are shown in Figure 2. Two main features are evident. First, the more mobile species are the Li⁺ ions. Second, the F[−] and Be²⁺ ions have very similar diffusion coefficients. These results are consistent with a picture of the structure for the liquid as a network of BeF₄^{2−} species, while Li⁺ cations move relatively freely around it, a picture we will examine more closely below.

For the present, we note that these diffusion coefficients give a Nernst–Einstein conductivity, which is in good accord with the full conductivity calculated above (see Figure 2); the ratio $\lambda/\lambda^{\text{NE}}$ is only 1.04 at this (67–33) composition and rises to 1.44 for the (50–50) one. This observation is significant because our calculated diffusion coefficients differ from the experimental ones by more than 1 order of magnitude (10.5×10^{-5} and 16.0

$\times 10^{-5} \text{ cm}^2 \text{ s}^{-1}$, respectively, for lithium⁸ and fluorine⁹ in the LiF–BeF₂ (67–33) mixture at 873 K). Those experimental values were obtained by using the capillary reservoir technique and seem to be much too high to be compatible with the more readily measured values of the electrical conductivity. To illustrate this point, we have calculated values for the conductivity by using the experimental values for the Li⁺ diffusion coefficient, as if *only* the Li⁺ ion is a significant charge carrier. The results are illustrated in the second part of Figure 2, where they are compared to the real electrical conductivity measured experimentally (with which our calculated conductivity agrees well, see Figure 1). They clearly indicate that the conductivity is strongly overestimated by the experimental diffusion coefficient via these approximations. When the F[−] anions are also included, the difference is enormous. The experimental diffusion coefficients could only be consistent with the experimental conductivity if there was a huge breakdown in the Nernst–Einstein approximation, which, at least in our simulations, seems to hold quite well. The very high conductivity predicted with the experimental diffusion coefficients is primarily due to the extraordinarily high values measured for the value of D_{F^-} . Ohmichi et al. attributed this high value for this diffusion coefficient to the movement of fluoroberyllate anions, the exchange of fluorine between neighboring anions, and ion pair diffusion.⁹ But as the formation of BeF₄^{2−} anions and the exchange of fluorine between complexes are well established in our simulations (see below) and because we obtain a good prediction of the conductivity with our diffusion coefficients, we can conclude that the first two processes cannot explain such a high value. The role of ion pairing will be discussed below.

B. Viscosity. The shear viscosity of a liquid can be calculated as the time integral of the shear stress autocorrelation function:

$$\eta = \frac{\beta}{V} \int_0^\infty \langle \sigma_{\alpha\beta}(t) \cdot \sigma_{\alpha\beta}(0) \rangle dt \quad (6)$$

To get better statistics, the stress autocorrelation function is averaged over its five independent components (σ_{xy} , σ_{xz} , σ_{yz} , σ_{xx-yy} , $\sigma_{zz-xx-yy}$). The viscosity is then given by the plateau value of the running integral.

A comparison between experimental values from Cantor et al.⁵ and our results shows a good agreement across the composition range we have examined, as can be seen in Figure 3. The shape of the curve shows that the viscosity increases sharply when the BeF₂ fraction is increased beyond 33%. Such a behavior should be related to the network formation at those concentrations, which will be investigated further below.

III. Local Coordination and Network Formation in the LiF–BeF₂ Mixtures

In pure BeF₂, the cation coordination number is very close to 4, and snapshots of the liquid structure (vide infra) indicate a tetrahedral network with corner-sharing linkages (i.e., pairs of Be²⁺ ions linked by a single F[−]). The Li⁺ ion is also 4-fold coordinated in liquid LiF, but because of the lower charge, we would anticipate that the coordination of Li⁺ with F[−] is weaker than that of Be²⁺ so that the structure of the mixtures should be dominated by the coordination requirements of the Be²⁺ ion. The radial distributions shown in Figure 4 are consistent with this picture, and the value of the coordination number of each ion can be obtained by a simple integration:

$$n_{\alpha\beta} = \rho_\beta \int_0^{r_{\text{min}}} g_{\alpha\beta}(r) 4\pi r^2 dr \quad (7)$$

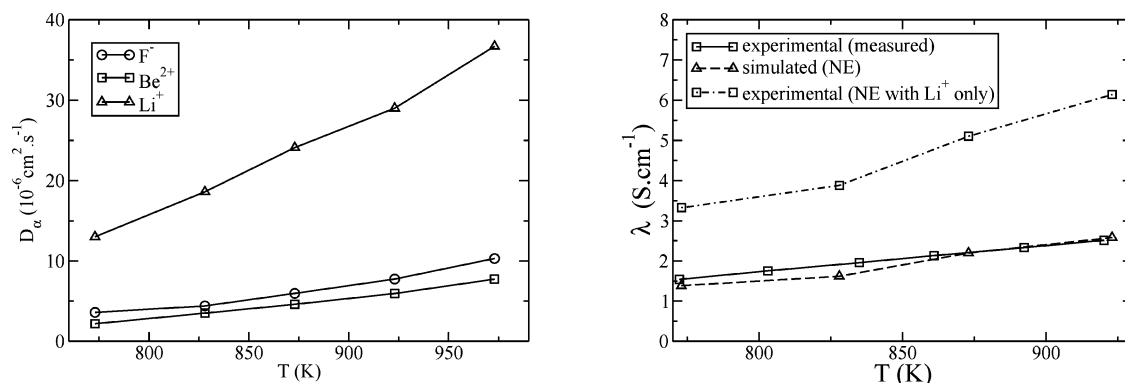


Figure 2. Left: Calculated diffusion coefficients as a function of temperature for the LiF–BeF₂ (67–33) system. Right: Measured and calculated electrical conductivity as a function of temperature for the LiF–BeF₂ (67–33) system.

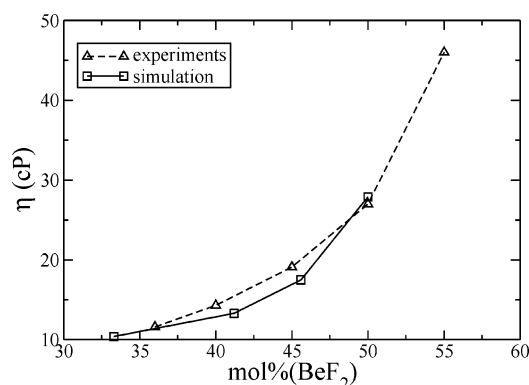


Figure 3. Experimental and simulated viscosities as a function of LiF–BeF₂ melt composition at 873 K.

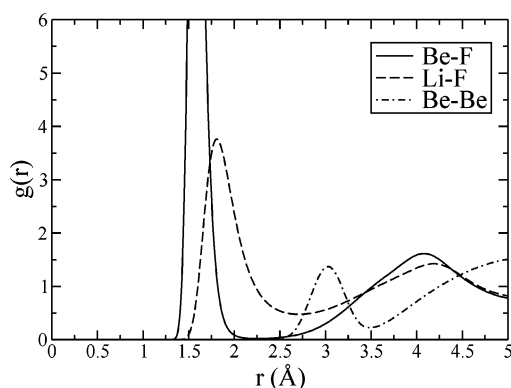


Figure 4. Radial distribution functions obtained for LiF–BeF₂ (67–33).

TABLE 1: Near-Neighbor Distances and First-Shell Coordination Numbers for the LiF–BeF₂ (67–33) Mixture.

ion pair $\alpha\beta$	$d_{\alpha\beta}(\text{\AA})$	$n_{\alpha\beta}$
F [−] –F [−]	2.61	11.3
F [−] –Be ²⁺	1.58	4.0
F [−] –Li ⁺	1.81	4.0
Be ²⁺ –Be ²⁺	3.03	0.9
Be ²⁺ –Li ⁺	3.07	6.9
Li ⁺ –Li ⁺	3.05	5.4

Here, r_{\min} is the distance corresponding to the first minimum of the RDF. All of the average near-neighbor distances and coordination numbers are listed in Table 1. Despite the fact that both Li⁺ and Be²⁺ cations are seen to retain a coordination number with F[−] of 4 across the composition range, this does not imply that their local structures are similar. Indeed, the first RDF peak for the Be–F pair is very sharp, with a high maximum and a very low minimum (nearly 0), whereas, for

TABLE 2: Distribution of Coordination Numbers in LiF–BeF₂ Mixtures

LiF–BeF ₂ , mole percent	Li ⁺ coordination number				Be ²⁺ coordination number		
	3	4	5	6	3	4	5
67–33 (%)	20.2	55.2	21.7	2.1	0.3	98.5	1.1
54–46 (%)	20.6	53.4	22.6	2.5	0.4	98.1	1.5
50–50 (%)	20.6	52.9	22.8	2.6	0.4	98.1	1.5

the Li–F pair, this peak is much broader and its minimum is quite high, suggesting relatively rapid exchange of coordinated F[−] ions with the bulk. Table 2 shows the distribution of coordination numbers of Be²⁺ and Li⁺ for different mixtures of LiF–BeF₂. It clearly shows that the Be²⁺ and the F[−] form BeF₄^{2−} tetrahedra, whereas no particular coordination complex emerges for Li⁺.

In principle, the BeF₂ network could be completely broken down by the addition of two equivalents of LiF to form a Li₂–BeF₄ mixture, which microscopically could be viewed as a melt consisting of Li⁺ and BeF₄^{2−} (fluoroberyllate) ions. For mixtures richer in BeF₂, there must be some linking of BeF₄^{2−} units because the Be coordination number remains 4 and there are less than four F[−] ions per Be²⁺. However, the transport coefficient data we discussed in the last section shows that even the Li₂BeF₄ mixture has a higher viscosity than one would expect for such a fully dissociated molten salt. Furthermore, X-ray diffraction data in this mixture¹⁰ shows a similar overall shape to that of pure BeF₂, which also suggests a persistence of the network structure. Because of the small electron numbers of Be²⁺ and Li⁺, the X-ray scattering is dominated by the F[−] correlations. The diffraction pattern predicted by the simulation model for the mixtures gives a similar good agreement with the experimental one as that obtained for the pure liquid in the first paper.¹ We will discuss the structure beyond the first coordination shell further below.

A. Lifetime of the First Coordination Shell. A fundamental time scale that will affect the properties of these mixtures is the lifetime of the coordination shell around a Be²⁺ ion, that is, the time scale for a change in the identities of the F[−] ions which make up the first coordination shell. Figure 5 shows the distance between a given Be²⁺ ion and two F[−] ions, one of which (“F2”) is initially in its coordination shell: in this time interval, we see it leaving the BeF₄^{2−} tetrahedron and its replacement by the other one nearly simultaneously. The Be–F distance is nearly constant, while the fluorine is in the coordination shell of the beryllium and then it increases very quickly and fluctuates more extensively when it leaves it. We can establish a time scale for an event of this kind by using the cage correlation function¹¹ that determines the rate at which the identities of the

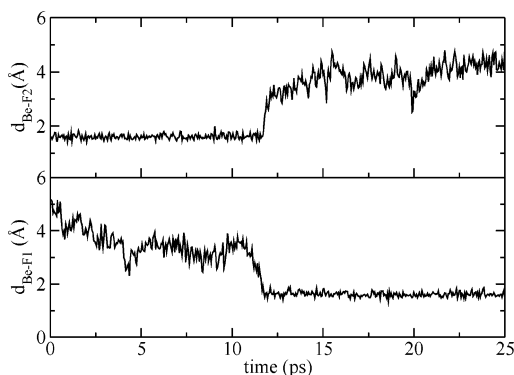


Figure 5. Distance between one Be and two different F atoms as a function of time.

ion in the coordination shell of a given ion change. This quantity is a useful tool to determine the lifetime of a coordination complex. The usual way to define this lifetime¹² is as the time needed for $(1 - 1/e)$ th of the coordination complexes to change the identity of at least one of their members, i.e., the time for which the cage correlation function takes the value of $1/e$. Figure 6 is a plot of this function for the LiF–BeF₂ (67–33) mixture at several temperatures. The corresponding lifetimes have been extracted and are shown as a function of temperature in the second part of Figure 6. The values for the other compositions studied at 873 K are nearly the same as those for the (67–33) mixture; they are also shown on Figure 6. This shows that the formation of BeF₄²⁻ entities is not dependent on the Li⁺ concentration; they appear to be well-defined entities that can be invoked in a discussion of the structure across a broad composition range.

B. Vibrational Dynamics of the Fluoroberyllate Ions.

Infrared and Raman spectra¹³ of the LiF–BeF₂ mixtures show discrete bands attributed to the vibrations of the BeF₄²⁻ ions. By adapting the method introduced by Pavlatou et al.,¹⁵ we can calculate densities of states associated with the symmetry coordinates of the tetrahedral BeF₄²⁻ units and compare them with the spectroscopic observations; in so doing, we both validate the interaction potential as concerns the Be–F interactions and also contribute to an understanding of the origin of the features in the experimental spectra.¹² For a tetrahedral molecule, vibrational normal coordinates ν_1 (A_1 , symmetric stretch), ν_2 (E , bend), ν_3 (F_2 , asymmetric stretch), and ν_4 (F_2 , bend) are expected. We may obtain velocities associated with

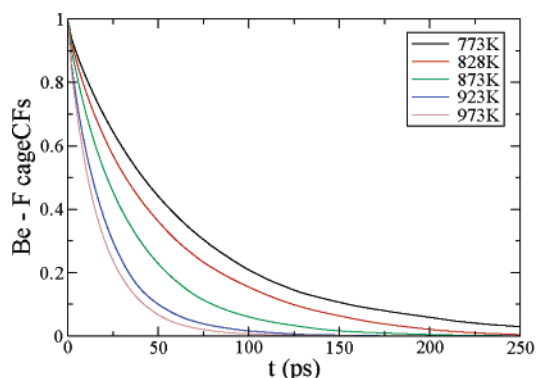


Figure 6. Left: Be–F cage correlation functions for LiF–BeF₂ (67–33) at several temperatures. Right: Lifetime of the Be²⁺ coordination shell for LiF–BeF₂ mixtures as a function of temperature.

TABLE 3: Vibrational Frequencies Observed in the Raman Spectra¹³ and in the Simulated Tetrahedral Normal Mode Vibrational DOS of LiF–BeF₂ Melts

75–25 exp (823 K)	75–25 md (1073 K)	66–34 exp (813 K)	67–33 md (873 K)	48–52 exp (752 K)	50–50 md (873 K)
235	236		253		236
375	371	365	371	371	
550	573	540	573	480	590
795	791	790	809	820	809

the symmetry coordinates of each BeF₄²⁻ unit. For example, for the symmetric stretching motion

$$V_A^i = \sum_{i\alpha=1-4} v_{i\alpha}^{\parallel} \quad (8)$$

where i labels the Be²⁺ of a complex, $i\alpha$ the four fluoride anions contained in the tetrahedra, and $v_{i\alpha}^{\parallel}$ is the projection of the relative velocity of $i\alpha$ along the $i \rightarrow i\alpha$ bond. Similar expressions may be written down for the velocities of the other symmetry coordinates.¹⁵ The density of states (DOS) is then obtained by a Fourier transform of the corresponding velocity autocorrelation function:

$$\text{DOS}_A(\omega) = \mathcal{R} \int_0^\infty e^{i\omega t} \langle V_A^i(t) \cdot V_A^i(0) \rangle dt \quad (9)$$

The DOS obtained for the LiF–BeF₂ (67–33) mixture are displayed in Figure 7. Strong features are observed, and at this

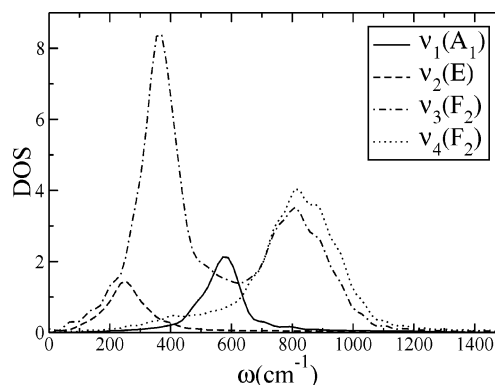
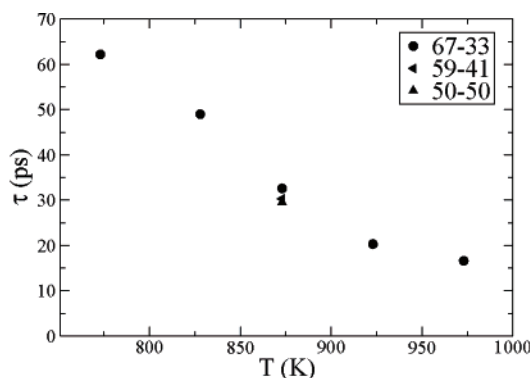


Figure 7. Tetrahedral normal mode vibrational DOS spectra for LiF–BeF₂ (67–33).

composition, the technique has achieved a good separation of the different modes, with the exception of ν_4 , to which both modes of F_2 symmetry appear to contribute. The peak frequencies can be compared to the shifts obtained in the Raman spectra.



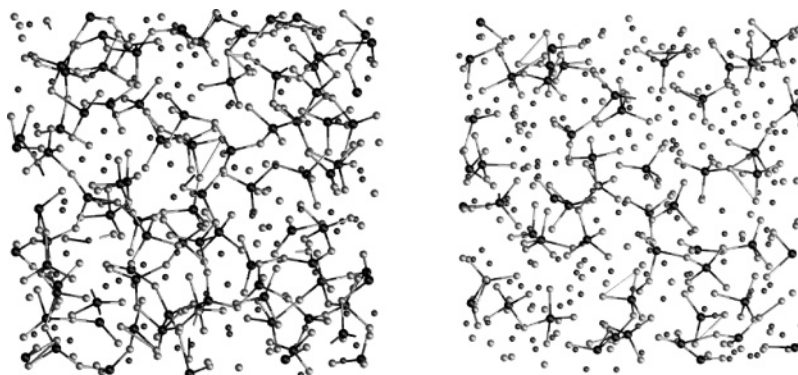


Figure 8. Snapshots of the simulation box for LiF–BeF₂ (50–50) at 873 K (left) and LiF–BeF₂ (75–25) at 1073 K (right), indicating the persisting Be–F network. Black: Be atoms; gray: Li atoms; silver: F atoms. Bonds are drawn for Be–F pairs separated by less than 2.3 Å.

All of the values are collected in Table 3. It shows that there is a good agreement for the LiF–BeF₂ (75–25) and (67–33) mixtures, where we might expect a relatively high proportion of isolated fluoroberyllate ions, but the agreement becomes worse for compositions richer in BeF₂, where these ions are more strongly coupled together in a network. The low-frequency vibrations (of *E* and *F*₂ symmetry) that we observe no longer appear as discrete bands in the Raman spectra, and bands at higher frequency than can be accounted for by fluoroberyllate normal modes are obtained experimentally. This indicates that the coupling of the BeF₄^{2−} units is having a significant effect on the spectra. A better approach to comparing the spectra with the simulation would be to calculate the full polarizability correlation function, as has been done for rare earth chlorides.¹² This will be the subject of future work.

IV. Network Formation and Speciation

A. Formation of Be–F–Be Bonds. As we have discussed above, several viewpoints indicate the existence of a network structure in the mixtures even down to the Li₂BeF₄ composition. Figure 4 shows a relatively sharp peak in the Be–Be radial distribution function at a distance of 3 Å, which is less than the length of two Be–F “bonds”, indicating pairs of Be ions linked by common F[−] ions. Three types of F[−] sharing between two tetrahedra can exist: two BeF₄ tetrahedra can share a corner, an edge, or a face (i.e., the two cations share 1, 2, or 3 common F[−] ions in their coordination shells). A geometrical criterion can be used to distinguish the nature of the linkages actually adopted. We chose to define a Be–F–Be bond when two Be–F and the corresponding Be–Be distances are shorter than the corresponding RDF minima; from this, the number of F[−] anions shared by any pair of cations can be counted. For all of the mixtures, even those richer in BeF₂, we obtained a negligible quantity of edge-sharing tetrahedra (less than 1%) and no face sharing. We can then conclude that the network is formed almost exclusively of corner-sharing tetrahedra. Snapshots of the ionic positions for two different (50–50 and 75–25) mixtures are shown in Figure 8, where ions that are closer than the first minimum of the Be–F RDF have been connected by “bonds”. In the 50–50 mixture, the existence of the tetrahedral network is clear; in the 75–25, an extended network no longer exists, but the liquid still cannot be described as a mixture of independent BeF₄^{2−}, F[−], and Li⁺ ions as might be expected (because the F[−]/Be²⁺ ratio is now 5). By extending the analysis of the linkages between ions described above, we can calculate the proportions of different polynuclear ionic species present in the melt such as Be₂F₇^{3−} and even of Be₃F₁₀^{4−}. A Be²⁺ that is linked to one other Be²⁺, according to the above criterion, is

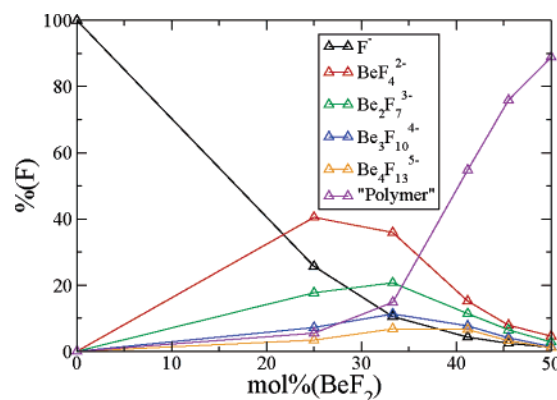


Figure 9. Percentage of F atoms involved in various species observed in the system as a function of composition; “polymer” means a cluster with a Be nuclearity greater than 4, whereas F[−] implies that the ion is coordinated only to Li⁺.

at the end of a chain, whereas one with a connectivity of two is in the middle of a chain. By walking along a chain of connected cations, we can determine the nuclearity of the species present. Even in the 75–25 mixture, the number of Be₂F₇^{3−} and Be₃F₁₀^{4−} is far from negligible. This result is in agreement with Baes’s polymer model for LiF–BeF₂ mixtures;³ the main difference being that Baes considered that edge sharing was not negligible. The composition of the system for the various compositions studied is given on Figure 9.

B. Lifetimes of the Network Connectivity. To evaluate the lifetime of the Be–F–Be bonds, we studied the Be–Be cage correlation functions for the various mixtures. A Be ion is considered linked to another if it is closer than the position of the first minimum in the Be–Be radial distribution function (Figure 4) at 3.5 Å, and the Be–Be cage correlation function is a measure of the time for such a linkage to break. This function is plotted in Figure 10 for three compositions of the melt. The figure shows that the Be–F–Be “bond” breakage time is not strongly dependent on composition, despite the fact that the proportions of Be₂F₇^{3−}, Be₃F₁₀^{4−}, etc. are changing quite strongly across this range of compositions, as shown in Figure 9. Because a linked pair of Be ions are almost invariably joined by a single F[−] ions and involves two Be–F bonds, the Be–F–Be bond breakage rate is greater than the rate of breakage of a single Be–F bond, which itself may be deduced from the Be–F cage correlation function. This simple picture suggests that we may use the Be–Be cage relaxation time as a time scale for major structural relaxation (by bond breakage) of the clusters and network in the melts.

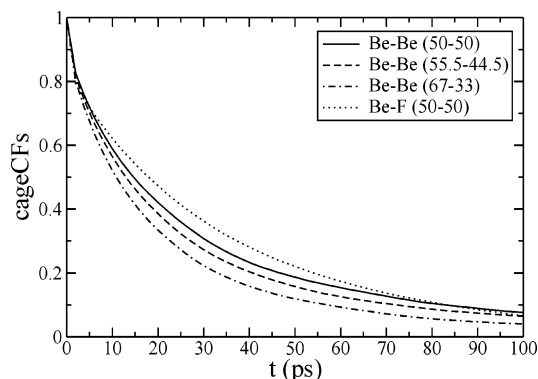


Figure 10. Be–Be cage correlation functions for LiF–BeF₂ (67–33) and (50–50) mixtures at 873 K.

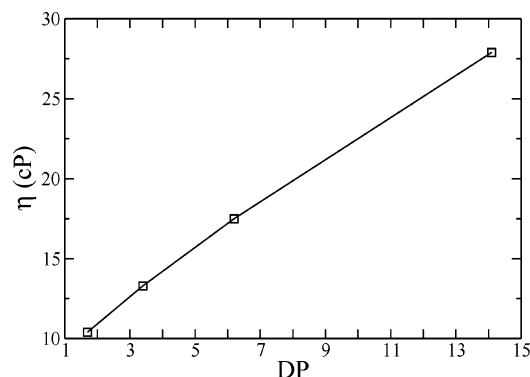


Figure 11. Viscosity of the LiF–BeF₂ melts at 873 K as a function of the degree of polymerization.

V. The Influence of the Network on the Transport Properties

In this section, we revisit the behaviors of the viscosity and the conductivity across the composition range to explore their relationship to the emerging network structure that was uncovered in the previous section.

A. Network Effect on the Viscosity. Figure 11 shows a plot of the shear viscosity versus the degree of polymerization of the system at each composition, and the data has been plotted for the 873 K isotherm. The degree of polymerization is defined as the mean number of Be ions per cluster species at the given composition. We recall (Figure 3) that the viscosity shows a strong increase as the amount of BeF₂ in the mixture increases, and this is caused by a rapid increase in the relaxation time of the stress tensor. In a phenomenological description, the viscosity is written as the product of a shear modulus (the resistance to strain in the absence of relaxation) and the structural relaxation time, and the shear modulus shows only very weak compositional and temperature dependence. The figure shows that when the viscosity is plotted against the degree of polymerization, the dependence is nearly linear and suggests that the relaxation of the shear stress is primarily affected by the structural relaxation of the network.

In Figure 12, we pursue this connection further by examining the relationship between the structural relaxation time of the melt and the various correlation times we have introduced to characterize the microscopic events that are occurring in the fluids. The figure shows the running integral of the stress tensor, normalized by its long time limit (the viscosity) for the Li₂BeF₄ and LiBeF₃ melts, and the substantial increase in the structural relaxation time as the melt becomes more concentrated in BeF₂ is apparent. We also compare these integrals with the Li–F and Be–F cage correlation functions, which, as we have

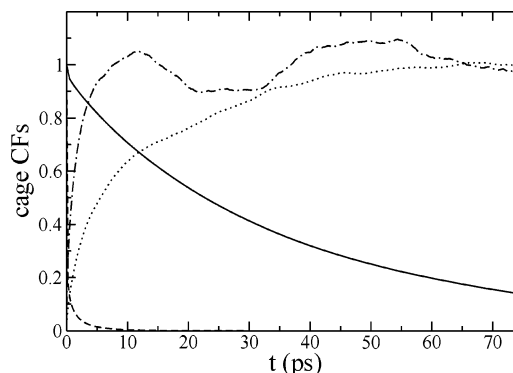


Figure 12. The stress tensor integrals (normalized to their long-time value) of the Li₂BeF₄ (dash–dot) and LiBeF₃ (dots) melts at 873 K are compared to the cage correlation functions for Li–F (dashed line) and Be–F (full) interactions.

already seen, do not themselves depend strongly on the mixture composition. In the dilute mixture, the structural relaxation time begins to approach that of the Li–F function, suggesting that, in this mixture (where the dominant Be-containing species are the small isolated ions BeF₄^{2−} and Be₂F₇^{3−}), the fluid can relax through the relative motion of ions in the LiF “solvent” without disrupting the Be–F coordination polyhedra (a similar effect was noted in dilute solutions of polyvalent chlorides¹⁴). On the other hand, when an extended network begins to form, as in LiBeF₃, it is necessary for the network configuration to relax and the time scale for the breakage of the linkages in the network is indicated, as discussed above, by the Be–F cage relaxation.

In technological applications, it is useful to work close to the eutectic composition, where operating temperatures can be quite low and the corrosiveness of the melt is consequentially reduced. However, the eutectic composition is in the régime where the viscosity is increasing rapidly as BeF₂ is added, which is an undesirable feature. The findings reported here suggest that it would be useful to add network-breaking cations such as heavier alkali fluorides to reduce the degree of polymerization of the network at the eutectic.

B. Stokes–Einstein Breakdown. This shift in character of the structural relaxation is also manifested by a decoupling of the Li⁺ diffusion from the viscosity. In dissociated fluids, including simple melts,¹⁶ the Stokes–Einstein relationship

$$D = \frac{k_B T}{4\pi\eta a} \quad (10)$$

gives a good guide to the connection between diffusion coefficient and viscosity, where a has been found to be close to the crystallographic radius of the ion,¹⁶ whereas polyvalent cations in alkali halides diffuse as if part of a coordination complex¹⁴ and a is close to the size of the complex. Correspondingly, in the more dilute (33%) mixture of BeF₂ in LiF, we find $a_{\text{Be}} \sim 2.2$ Å, much larger than the crystallographic radius but close to the position of the first minimum in the Be–F RDF (Figure 4), whereas $a_{\text{Li}} = 0.41$ Å, which is even smaller than the Li⁺ crystallographic radius (0.7 Å). As the mixture becomes more concentrated in BeF₂, the effective radius of Li⁺ becomes even smaller (0.19 Å in LiBeF₃), indicating that the diffusive motion of the Li⁺ ion becomes decoupled from the dominant structural relaxation process when the extended network begins to form.

C. Li⁺ Ions Dominate the Conductivity. It is possible to recast eq 1, which expresses the relationship between the conductivity and the net displacement of all the ions of a given

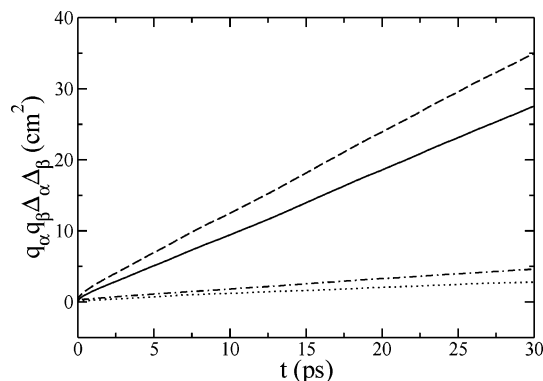


Figure 13. Decomposition of the mean-squared charge displacement into a contribution from Li⁺ ions and from the remainder, showing that the lithium ion motion dominates the conductivity (dashed line: total conductivity; full line: Li⁺ contribution; dashed-dotted: network contribution; dotted: Li⁺ displacement relative to the network).

species, to separate the contributions to the conductivity due to the motion of the Li⁺ ions and of the network:

$$\lambda = \frac{\beta e^2}{V} \lim_{t \rightarrow \infty} \frac{1}{6t} \{ q_{\text{Li}}^2 \langle |\Delta_{\text{Li}}(t)|^2 \rangle + \langle |\Delta_{\text{net}}(t)|^2 \rangle + 2q_{\text{Li}} \langle \Delta_{\text{Li}}(t) \cdot \Delta_{\text{net}}(t) \rangle \} \quad (11)$$

where

$$\Delta_{\text{net}}(t) = q_{\text{Be}} \Delta_{\text{Be}}(t) + q_{\text{F}} \Delta_{\text{F}}(t) \quad (12)$$

The three separate contributions are plotted together with the total mean-squared charge displacement in Figure 13. The figure emphasizes that the conductivity of the mixture is dominated by motion of the Li⁺ ions. As Figure 12 emphasizes, as the melt becomes more concentrated in BeF₂ and the viscosity begins to increase sharply, Li⁺ ions break free from their coordination cages on a time scale (the Li–F cage relaxation time) that becomes much more rapid than the structural relaxation time determining the viscosity, whereas in the dilute solutions, these time scales are more similar. From Figure 13, we can also show that the contribution of the Li⁺ net displacement relative to the network gives a positive contribution to the conductivity (dotted line). This excludes the possibility of formation of neutral Li₂BeF₄ ion pairs to account for the high diffusion coefficients measured experimentally.

VI. Conclusion

We have shown in this study how a simple model allows a complete study of BeF₂ mixtures with LiF. The model was parametrized purely from first principles, and the excellent agreement demonstrated between experimental and simulated properties opens up the way of predicting the behaviors of difficult-to-study fluoride melts from purely theoretical considerations. The only many-body effect included in the potential

is the anion polarization, which enabled us to perform long enough runs to get the dynamic properties of the systems. The polarization effects seem to be crucial in reproducing the properties of the networks that form in these melts and control their dynamical properties. The calculated electrical conductivities and viscosities agree very well with experimental results on the whole range of composition studied. This allows us to validate the values we obtained for the diffusion coefficient of the various ions in the melt and to conclude that the measured values of these quantities by Ohno et al. are much too high.

The structure of the LiF–BeF₂ mixtures can be depicted as a network of BeF₄^{2−} tetrahedral ions that are connected by their corners, even in the diluted Li₃BeF₅. The proportions of BeF₄^{2−}, Be₂F₇^{3−}, and higher polymers could be quantified. As the high viscosity obtained can be directly correlated to the size of the polymers present in the liquid, an eventual tuning of this property could be achieved by adding a proper amount of network-breaking cations in the liquid.

We have also shown that the Li⁺ cations can move quite independently from the fluoroberyllate network and that their motion can be decoupled from the viscosity. Consequently, the electrical conductivity stays quite high, even for the most viscous salt studied, LiBeF₃.

Acknowledgment. P.A.M. is grateful to the Université Pierre et Marie Curie for his appointment as Professor Invité which enabled this collaboration.

References and Notes

- (1) Heaton, R. J.; Brookes, R.; Madden, P. A.; Salanne, M.; Simon, C.; Turq, P. *J. Phys. Chem. B* **2006**, *110*, 11454.
- (2) Madden, P. A.; Heaton, R. J.; Aguado, A.; Jahn, S. J. *Mol. Struct. (THEOCHEM)*. To be published.
- (3) Baes, C. F. *J. Solid State Chem.* **1970**, *1*, 159.
- (4) Romberger, K. A.; Braunstein, J.; Thomas, R. E. *J. Phys. Chem.* **1972**, *76*, 1154.
- (5) Cantor, S.; Ward, W. T.; Moynihan, C. T. *J. Chem. Phys.* **1960**, *50*, 2874.
- (6) Robbins, G. D.; Braunstein, J. *Molten Salt Reactor Program, Semiannual Progress Report*; Report ORNL-4344; Oak Ridge National Laboratory: Oak Ridge, TN, 1968. Robbins, G. D.; Braunstein, J. *Molten Salt Reactor Program, Semiannual Progress Report*; Report ORNL-4449; Oak Ridge National Laboratory: Oak Ridge, TN, 1969. Robbins, G. D.; Braunstein, J. *Molten Salt Reactor Program, Semiannual Progress Report*; Report ORNL-4548; Oak Ridge National Laboratory: Oak Ridge, TN, 1970.
- (7) Castiglione, M. J.; Madden, P. A. *J. Phys.: Condens. Matter* **2001**, *13*, 9963.
- (8) Iwamoto, N.; Tsunawaki, Y.; Umesaki, N.; Ohno, H.; Furukawa, K. *J. Chem. Soc., Faraday Trans. 2* **1979**, *75*, 1277.
- (9) Ohmichi, H.; Ohno, H.; Furukawa, K. *J. Phys. Chem.* **1976**, *80*, 1626.
- (10) Vaslow, F.; Narten, A. H. *J. Chem. Phys.* **1973**, *59*, 4949.
- (11) Rabani, E.; Gezelter, J. D.; Berne, B. J. *J. Chem. Phys.* **1998**, *109*, 4695.
- (12) Glover, W. J.; Madden, P. A. *J. Chem. Phys.* **2004**, *121*, 7293.
- (13) Toth, L. M.; Bates, J. B.; Boyd, G. E. *J. Phys. Chem.* **1973**, *77*, 216.
- (14) Brookes, R.; Davies, A.; Ketwaroo, G.; Madden, P. A. *J. Phys. Chem. B* **2004**, *109*, 6485.
- (15) Pavlatou, E. A.; Madden, P. A.; Wilson, M. J. *J. Chem. Phys.* **1997**, *107*, 10446.
- (16) Morgan, B.; Madden, P. A. *J. Chem. Phys.* **2004**, *120*, 1402.